Journal of Sol-Gel Science and Technology (2023) 105:848–856
https://doi.org/10.1007/s10971-022-06003-8

ORIGINAL PAPER: NANO-STRUCTURED MATERIALS (PARTICLES, FIBERS, COLLOIDS, COMPOSITES, ETC.)

Electrospun boron-containing mullite micro/nanofibers derived from monophasic sol: effects of sol concentration on morphology and microstructure

Xiaolei Song[1] · Jianxiang Xu[1] · Ying Song[1] · Rui Chen[1] · Yang Gao[1] · Yunzhu Ma[2] · Wensheng Liu[2]

Received: 15 September 2022 / Accepted: 21 November 2022 / Published online: 10 December 2022

Abstract

Continuous mullite fibers with ultrafine diameters and good thermal stability are an ideal candidate to be used to prepare ceramic-based aerogels, sponges, or composites. In the present work, boron-containing mullite micro/nanofibers with the molar ratio of Al/Si/B = 3/1/1 were fabricated using monophasic precursor sols with different concentrations (15–37.5%) by electrospinning. Basic aluminum acetate (BAA) and tetraethyl orthosilicate (TEOS) were used as the raw materials. It was found that with increasing sol concentration, the reaction rates of hydrolysis and polymerization were reduced, and the chemical homogeneity of the precursor sols decreased. Besides, the viscosities of the spinning solutions increased, which was assigned to be the determining factor that led to the increasingly thicker precursor fibers. Meanwhile, the crystallization temperatures decreased and the grain sizes increased for the sintered fibers. The main reason for this was that amorphous SiO_2, which could delay the reaction between Al_2O_3 and B_2O_3 and hinder the movement of grain boundaries, was distributed more evenly.

Graphical abstract

Effects of sol concentration on morphology, crystallization temperatures and phase composition of electrospun boron-containing mullite micro/nanofibers derived from monophasic sol.

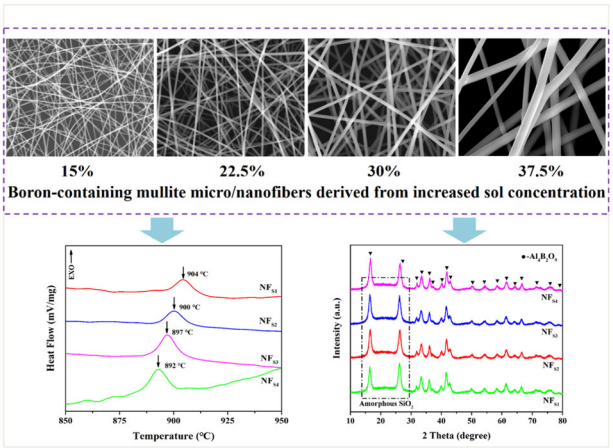

✉ Xiaolei Song
songxiaolei@ccut.edu.cn

✉ Ying Song
songying@ccut.edu.cn

✉ Yang Gao
gaoyang_0226@163.com

[1] Key Laboratory of Advanced Structural Materials, Ministry of Education, Changchun University of Technology, Changchun 130012, China

[2] State Key Laboratory of Powder Metallurgy, Central South University, Changsha 410083, China

Keywords Mullite micro/nano-fibers · Electrospinning · Sol concentration · Alumina borate

Highlights

- Electrospun boron-containing mullite micro/nanofibers were prepared using monophasic precursor sols.
- The fiber derived from precursor sols with higher concentration possessed larger diameters.
- High sol concentration led to low crystallization temperatures and large grains of the fibers.

1 Introduction

One-dimensional ceramic nanomaterials with outstanding mechanical and thermal properties, such as Al_2O_3 nanotubes, SiO_2 nanofibers, TiO_2 nanofibers, ZrO_2 nanofibers, SiC nanowires, *etc*., are drawing increasing attention due to their successful application in producing high-performance and multifunctional ceramic-based aerogels, sponges, and composites [1–4]. Mullite fibers in micro/nano scale, which possess the low expansion coefficient, low thermal conductivity, high creep resistance and high structural stability under high temperature conditions [5–7], are also a kind of promising raw materials used to prepare ceramic products with superior properties.

Electrospinning has become one of the most promising techniques in the fabrication of various kinds of ceramic micro/nanofibers in the past two decades [8–10]. Using a combination of electrospinning and the sol-gel method, mullite micro/nanofibers have been successfully fabricated [11–17]. As introduced by these literatures, precursor sols were normally synthesized using aluminum nitrate, aluminum isopropoxide or aluminum chloride as the alumina sources, and using tetraethyl orthosilicate as the silica source. Aluminum and silicon were hydrolyzed simultaneously according to their preparation process. In general, this is a typical route in synthesizing monophasic mullite sol [18]. The formation temperatures of mullite derived from this sol were normally below 1000 °C, which would result in the rapid growth of grains at high temperatures and might eventually affect the applications of the mullite nanofibers. For example, Wu et al. [11, 12] fabricated electrospun mullite nanofibers with an average diameter of about 200 nm at 1200 °C. Although the fibers were continuous, the crystal grains were relatively large (~100 nm), which would make the fiber mat easily destroyable under mechanical contact stress.

An effective method to improve the thermal stability of the nanofiber is to introduce the second phase. In our previous work, 14 wt. % B_2O_3 was introduced into electrospun monophasic mullite nanofibers with an Al_2O_3:SiO_2 mol ratio of 3:2 [19, 20]. The fabricated Al_2O_3-SiO_2-B_2O_3 nanofibers had better thermal stability than those pure monophasic mullite nanofibers. An important reason for this was that Al_2O_3 reacted with B_2O_3 to form the phase $Al_4B_2O_9$ first, instead of transforming to γ-Al_2O_3 or reacting with SiO_2 to form mullite during the calcination process. SiO_2 was in the amorphous state, its existence favored to hinder the growth of crystal grains and promote the closure of tiny voids and cracks, and consequently, thermally stable nanofibers were obtained.

The well mixing of the mullite sol and polymer solution can acquire spinning solutions suitable for electrospinning. Once the properties of one component change, the properties of the spinning solution change accordingly, and finally the electrospinning process and the fiber morphology will be affected [21–23]. During the sol preparation process, the concentration has significant influence on the degree of hydrolysis and polymerization and can lead to different physicochemical properties. However, most of the researches have focused on the effects of polymer dosage on the morphology and microstructure of mullite nanofibers [11, 15, 16, 24], and little attention has been paid to the influences of sol concentration.

On the basis of the above discussion, boron-containing mullite micro/nanofibers were fabricated using sols with different concentrations via electrospinning method in this paper. Basic aluminum acetate (BAA) and tetraethyl orthosilicate (TEOS) were used as the starting materials. PVP was used as the polymer additive. The influences of sol concentration on the morphology and microstructure of the fibers were investigated in detail.

2 Experimental

2.1 Sample preparation

BAA ($Al(OH)_2(OOCCH_3)\cdot 1/3H_3BO_3$, Strem, USA) and TEOS (Xilong, China) were used as raw materials. Absolute ethanol (Hengxing, China) and deionized water were used as the solvents. The molar ratio of Al:Si:B of boron-containing mullite nanofibers was designed to be 3:1:1. As listed in Table 1, the two raw materials and two solvents were mixed with different mass fractions. After stirring at 40 °C for 8 h, four precursor sols (labeled S1, S2, S3, and S4, respectively) with different concentrations were acquired.

Table 1 Dosages of raw materials and basic characterization of precursor sols

Sample	Dosage (wt. %)				Concentration (%)	pH	Particle size (nm)	Dry solid content (%)
	BAA	TEOS	H_2O	EtOH				
S1	10	5	42.5	42.5	15.0	4.90	6.8	10.64
S2	15	7.5	38.75	38.75	22.5	4.79	38.1	16.50
S3	20	10	35	35	30.0	4.67	77.8	22.10
S4	25	12.5	31.25	31.25	37.5	4.60	122.4	27.75

PVP (Mw = 1,300,000, Bodi, China) was dissolved in alcohol to acquire a 15 wt. % solution. The mass ratio of the PVP solution and precursor sols was set to be 1:1. Homogeneous spinning solutions were prepared after stirring the mixtures at room temperature for 1 h.

Afterward, each spinning solution was transferred into a syringe equipped with a metallic needle. Electrospinning was conducted using a voltage of −6.0 kV, a feeding rate of 0.25 ml/h and a distance of 12 cm between the needle tip and grounded collector. The collected precursor fibers were dried at 40 °C for at least 3 h. The fibers were then heated to 900 and 1200 °C in an air circumstance with a heating rate of 10 °C/min and maintained for 1 h at the end temperatures. In the following discussion, the electrospun fibers were marked as NF_{S1}, NF_{S2}, NF_{S3}, and NF_{S4}, accordingly.

2.2 Characterization methods

For the spinning solutions, the viscosities were recorded using a NDJ-9TE digital viscometer (Jitai, China), the conductivities were obtained by a DDB-303A digital conductivity meter (Leici, China), and the surface tensions were acquired using a ELB-ZL surface tension meter (Enlab, China). All of these data were measured at 25 °C.

The fiber morphology was observed by a JSM-IT500 scanning electron microscope (SEM, JEOL, Japan). Fiber diameters were calculated using image analysis software (Image J). The chemical structure of the precursors was investigated by Fourier transform infrared (FT-IR) absorption spectra measured using a NicoletIS50 spectrometer (Thermofisher, USA). The ceramic yields and crystallization temperatures of the precursor fibers were acquired using the thermogravimetric and differential scanning calorimetry (TG-DSC) method performed on an STA-449C thermal analyzer (Netzsch, Germany) at a heating rate of 10 °C/min and an end temperature of 1000 °C in the air. The phase composition of the mullite fibers were determined by X-ray powder diffraction (XRD) and the data were detected by a D/max2500 vpc diffractometer (Rigaku, Japan) using Cu$K\alpha$ in the region of $10 < 2\theta < 80°$. The crystal grains were observed using a Talos F200s (FEI, USA) transmission electron microscope (TEM).

3 Results and discussion

3.1 Precursor sols

BAA and TEOS in the mixed solvent were hydrolyzed based on the following equations [25]:

$$Al(OH)_2Ac + H_2O \rightarrow Al(OH)_3 + HAc \quad (1)$$

$$Si(OC_2H_5)_4 + nH_2O \rightarrow (C_2H_5O)_{4-n}Si(OH)_n + nC_2H_5OH \quad (2)$$

where the n values in Eq. (2) ranged from 0 to 4. Because of the HAc formed through Eq. (1) and the boric acid introduced by BAA, the acidic condition developed. It facilitated the condensation polymerization between TEOS and its hydrolysates and the formation of polysiloxanes [25]:

$$Si(OC_2H_5)_4 + (C_2H_5O)_{4-n}Si(OH)_n \rightarrow (-O-Si-O-)_m + C_2H_5OH \quad (3)$$

Meanwhile, it was also expected that the condensation polymerization between BAA (or its hydrolysates) and the hydrolysates of TEOS occurred, for instance:

$$Al(OH)_2Ac + (C_2H_5O)_2Si(OH)_2 \rightarrow (-Al-O-Si-)_n \quad (4)$$

The linear products in Eqs. (3) and (4) were believed to be beneficial in improving the spinnability during the spinning process.

The basic characterization of the prepared mullite sols is also listed in Table 1. With the concentration increased from 15 to 37.5%, the pH values decreased from 4.9 to 4.6, the mean particle sizes increased from 6.8 to 122.4 nm, and the solid content increased from 10.64 to 22.75%. According to Eq. (1), more HAc would be generated when more BAA was used and hydrolyzed, thereby leading to a decrease in pH values. From the above equations, it could also be deduced that the amounts of colloidal particles increased. In this case, the Brownian movement of the particles weakened, which made the combination between nearby ones occur easily. This was the main reason for the increased particle sizes.

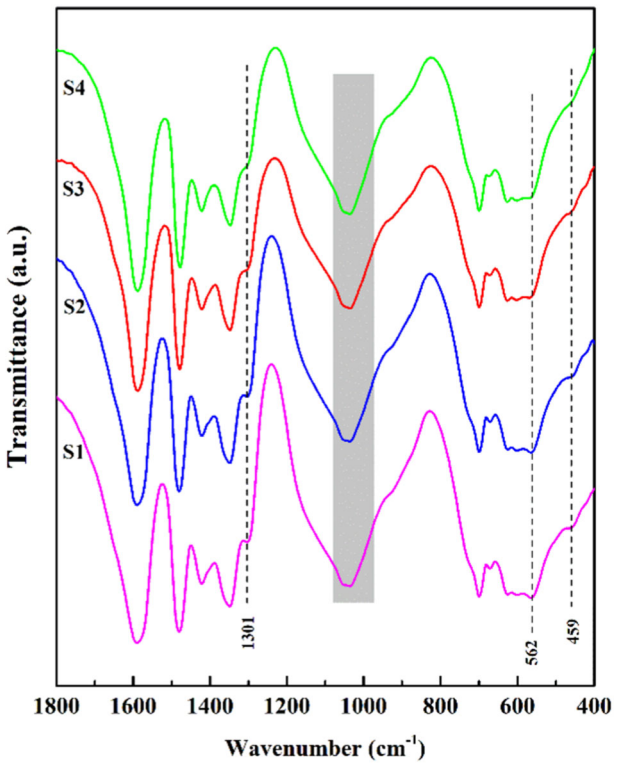

Fig. 1 FT-IR spectra of the dried precursor gels derived from sols with different concentrations

The FT-IR spectra of the precursor gels are displayed in Fig. 1. As could be seen, the locations and assignments of the absorption bands for the four samples were basically the same. However, the intensities of some absorption bands weakened when the sol concentration increased from 15 to 37.5%. Typically, shoulder peaks at 459 cm^{-1} were ascribed to stretching vibration in Al-OH and bending vibration in O-Si-O, absorption bands at 562 cm^{-1} assigned to stretching vibration of Al-O and stretching vibration in O-Si-O, bands appeared at 1301 cm^{-1} corresponded to vibrations of CH_2 groups, and broad absorption bands at 980–1080 cm^{-1} due to stretching vibration of Al-O-Si bend [18, 26, 27]. The variation of these bands indicated that the reaction rates of hydrolysis and polymerization in Eqs. (1 to 4) reduced, which finally led to a decrease in the chemical homogeneity of the precursor sols.

3.2 Spinning solutions

Figure 2 shows the viscosities, conductivities, and surface tensions of the spinning solutions. As clearly seen in Fig. 2a, the samples prepared using S1 to S4 had viscosities of 247.2, 408.8, 571.6 and 947.5 mPa·s, respectively. Such a variation was ascribed to the increase in the sizes and amounts of colloidal particles in the solutions. On one hand, colloidal particles could hinder PVP molecular movement due to the steric hindrance effect. On the other hand, the Al-OH bond or the Si-OH bond on the colloidal particles might react with the ketonic oxygen on the lateral chain of PVP to form hydrogen bonds. Once more colloidal particles appeared, their hindrance effect became stronger and more linkages between the particles and PVP molecule chains were generated. In this case, the larger viscous force was required for the slide of the PVP molecule chains, and consequently, the viscosities increased. In Fig. 2b, as the concentration varied from 15 to 37.5%, the conductivity increased steadily from 51.4 to 197.6 μS/m. The increased conductive ions and charged colloidal particles were responsible for this. While, as illustrated in Fig. 2c, the surface tensions for the solutions prepared by S1 to S4 were 25.1, 24.6, 22.4 and 19.8 mN/m, respectively. That was, the surface tension exhibited a slightly decreased trend at elevated concentrations. Definitely, this was caused by the increased content of solvent.

3.3 Fiber morphology

Figure 3 shows the SEM images of precursor fibers prepared using different sols. As observed, all the fibers exhibited continuous, smooth, and cylindrical features despite the fact that the concentrations of the precursor sols were different. An increased tendency of fiber diameters was found. The average diameter was about 535 nm for NF_{S1}, while it reached up to 2829 nm for NF_{S4}. To our knowledge, to acquire thinner electrospun fibers, a solution with low viscosity, high conductivity, and low surface tension was preferable [9, 21]. On considering the properties of the spinning solutions, it was concluded that the viscosities played a dominant role in affecting the diameters. Another often-ignored effect factor for the diameters of precursor micro/nanofibers was the gelation processes carried out during electrospinning [28]. Due to the lowest solvent content, the gelation speed of S4 was the fastest. Thus, the elongation of the fibers was impeded, although they were still under electrostatic repulsion.

The SEM images and diameter distribution histograms of mullite micro/nanofibers obtained at 900 °C are exhibited in Fig. 4. The fibers retained the continuous, smooth, and cylindrical morphology after sintering. Due to the decomposition of PVP and organics, the average diameters for the four samples decreased to 244, 415, 678 and 1247 nm, respectively. The diameter shrinking percentages (η) were calculated by the following equation:

$$\eta = \frac{D_1 - D_2}{D_1} \times 100\% \quad (5)$$

where D_1 and D_2 were the average diameters of the precursor fibers and sintered fibers. The calculated η values are displayed in Fig. 5. Fibers prepared using S1 had a η value of 54.39%, while those derived from S4 decreased

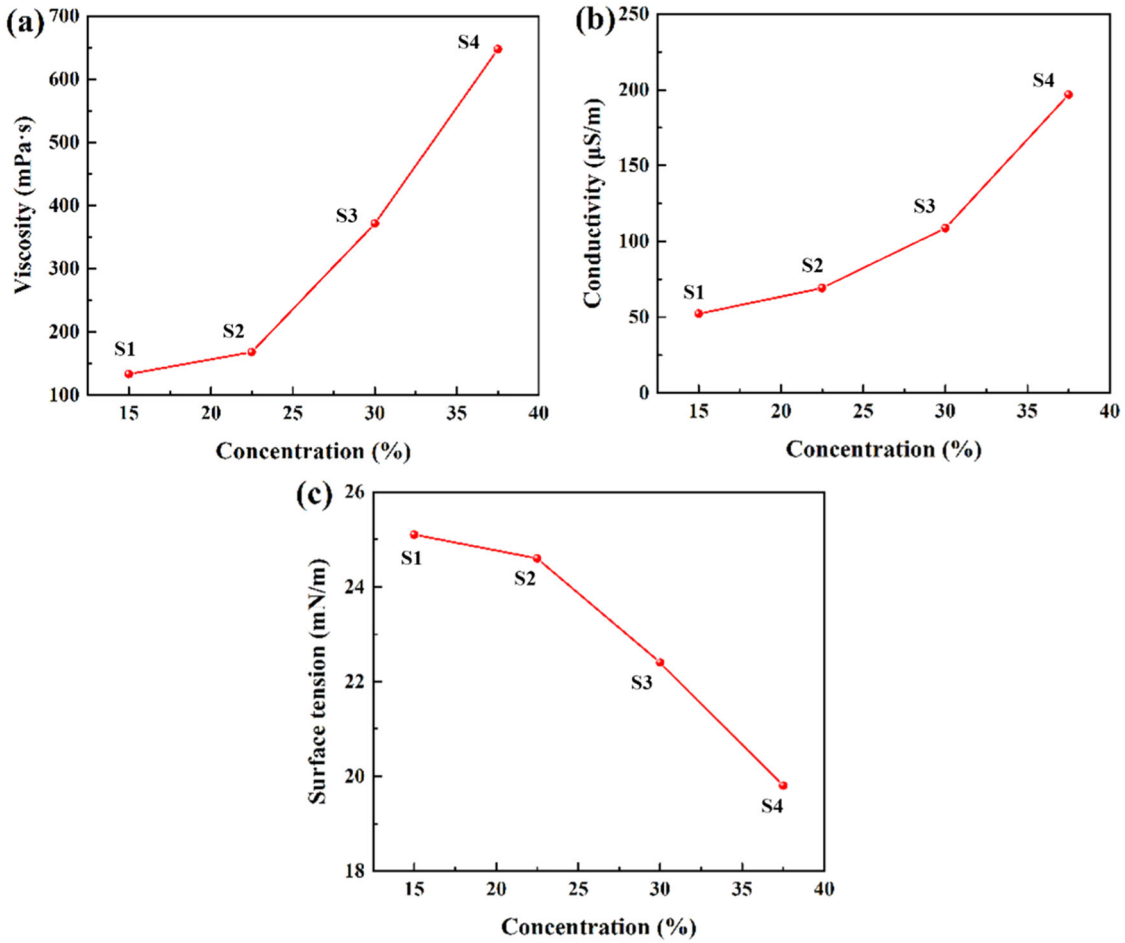

Fig. 2 **a** Viscosities, **b** conductivities, and **c** surface tensions of spinning solutions prepared using precursor sols of S1 o S4

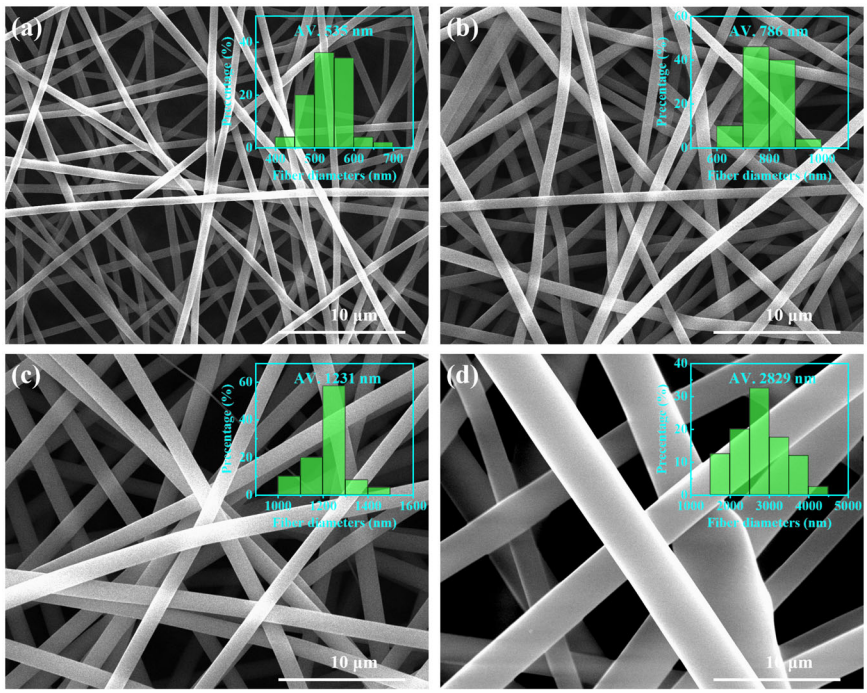

Fig. 3 SEM images of precursor micro/nanofibers: **a** NF_{S1}, **b** NF_{S2}, **c** NF_{S3} and **d** NF_{S4}. The insets display the diameter distribution histograms

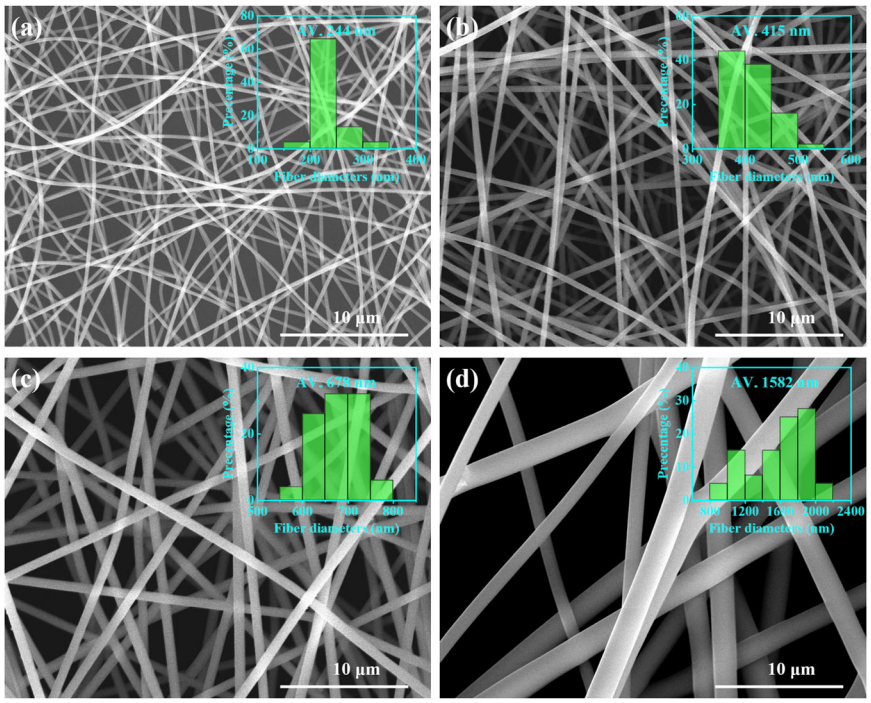

Fig. 4 SEM images of mullite micro/nanofibers after sintering at 900 °C: **a** NF_{S1}, **b** NF_{S2}, **c** NF_{S3} and **d** NF_{S4}. The insets display the diameter distribution histograms

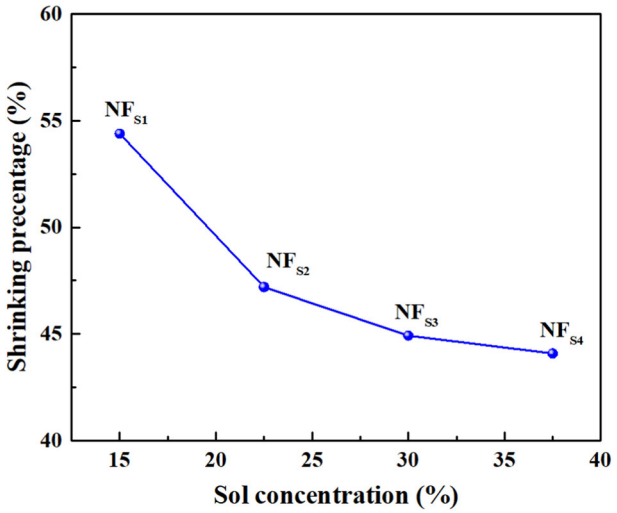

Fig. 5 Diameter shrinking percentages for mullite micro/nanofibers prepared using different sols after sintering at 900 °C

to 44.08%. It could be concluded from Table 1 that the PVP contents in precursor fibers decreased with the increase of sol concentration. The low PVP content certainly led to the small shrinking of fiber diameter.

3.4 Fiber microstructure

TG and DSC curves of precursor fibers prepared using different sols are displayed in Fig. 6. Figure 6a showed that the ceramic yields of the precursor NF_{S1}, NF_{S2}, NF_{S3} and NF_{S4} at 1000 °C were 28.54, 31.54, 33.60 and 35.31%, respectively. The lowest ceramic yield for NF_{S1} was attributed to the largest PVP content. The exothermic peaks in Fig. 6b at around 900 °C were assigned to the formation of $Al_4B_2O_9$ phase. Researchers once reported that the more PVP existed in precursors resulted in the higher crystallization temperatures for oxide ceramics [24, 29]. However, the present work showed an opposite rule. NF_{S1} crystallized at 904 °C, which was 12 °C higher than that of NF_{S4}. As discussed above, the sol with a high concentration presented a low chemical homogeneity. In this case, less SiO_2 hindered the reaction between Al_2O_3 and B_2O_3, and therefore the crystallization temperatures decreased with the increase of sol concentrations.

The XRD patterns of mullite micro/nanofibers prepared using different precursor sols after sintering at 900 and 1200 °C are displayed in Fig. 7. According to our previous works [19, 30], it was clear that the samples prepared at 900 °C were composed of the $Al_4B_2O_9$ phase (Card No. 47-0319) and amorphous SiO_2 (Fig. 7a). For $Al_4B_2O_9$ phase, the diffraction peaks at the 2θ of about 26° and 16° represent the crystal planes with d-spaces of 0.34 nm and 0.54 nm, respectively. As calculated, the intensity ratio ($I_{0.34}/I_{0.54}$) of the two diffraction peaks is 0.78. The $I_{0.34}/I_{0.54}$ values for mullite micro/nanofibers prepared at different temperatures are displayed in Fig. 8. As could be seen, the $I_{0.34}/I_{0.54}$ values for the sintered samples at 900 °C were all larger than 0.78. This demonstrated that solid solution occurred during the crystallization process since $Al_4B_2O_9$ was the only crystal phase. Most of the researches on ceramics in the Al_2O_3-SiO_2-B_2O_3 ternary system presented that B was in solid solution in

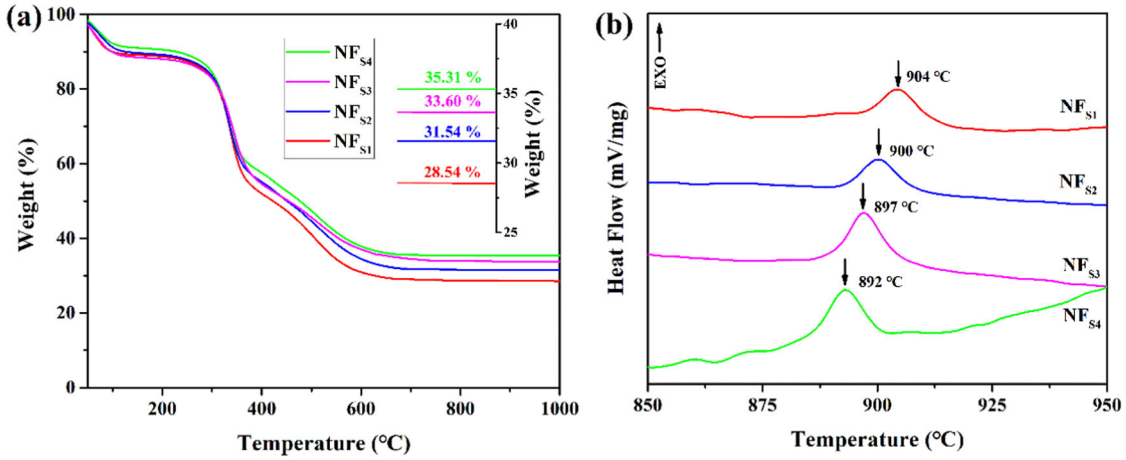

Fig. 6 **a** TG and **b** DSC curves of precursor fibers prepared using different sols

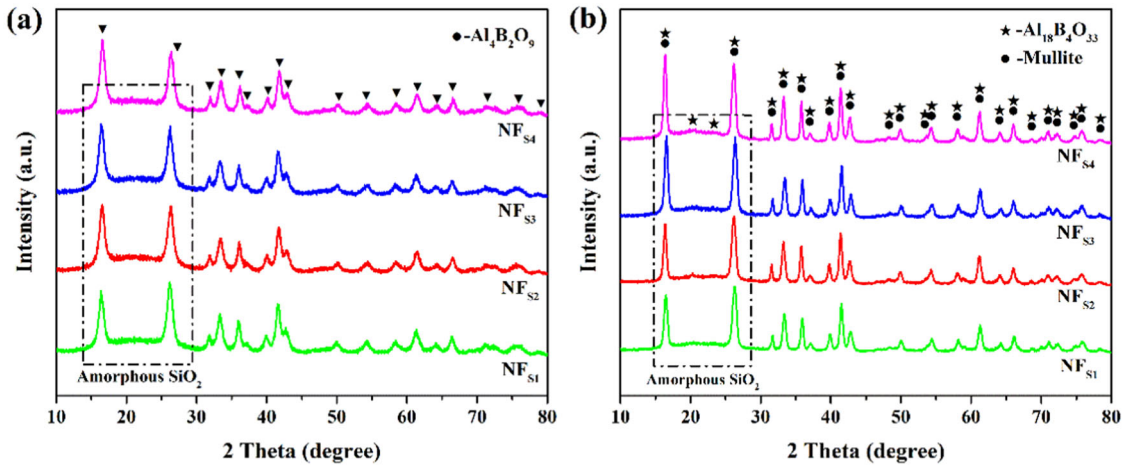

Fig. 7 XRD patterns of mullite micro/nanofibers prepared using different precursor sols after sintering at **a** 900 °C and **b** 1200 °C

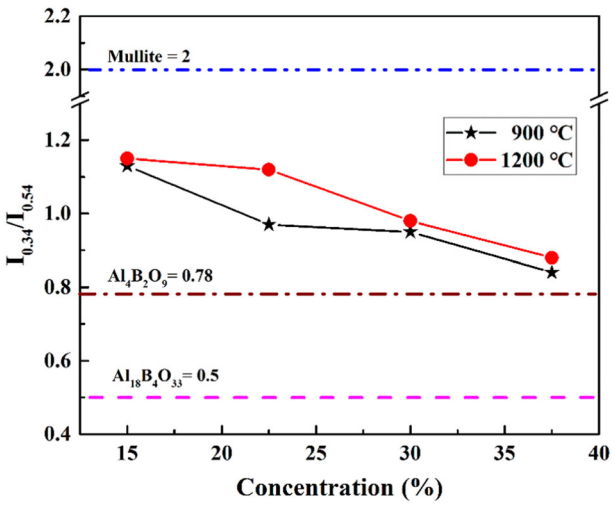

Fig. 8 $I_{0.34}/I_{0.54}$ values for mullite micro/nanofibers prepared at 900 and 1200 °C

Table 2 Lattice parameters and unit cell volumes of $Al_4B_2O_9$ for mullite micro/nanofibers prepared at 900 °C

Samples	a(Å)	b(Å)	c(Å)	V(Å^3)
NF$_{S1}$	7.59835	7.61577	2.82226	163.32
NF$_{S2}$	7.57979	7.59866	2.81989	162.42
NF$_{S3}$	7.57066	7.59781	2.81597	161.96
NF$_{S4}$	7.55594	7.57377	2.80949	160.78

mullite [31, 32]. Herein, we attributed the larger $I_{0.34}/I_{0.54}$ values to the incorporation of Si into the alumina borate structure. As is well known, the radium of Si^{4+} ion (0.041 nm) was larger than that of B^{3+} ion (0.02 nm). Once the substitution of Si^{4+} for B^{3+} occurred, the lattice parameters and unit cell volume of the $Al_4B_2O_9$ would increase. The lattice parameters and unit cell volumes of $Al_4B_2O_9$ for mullite fibers prepared at 900 °C are listed in Table 2.

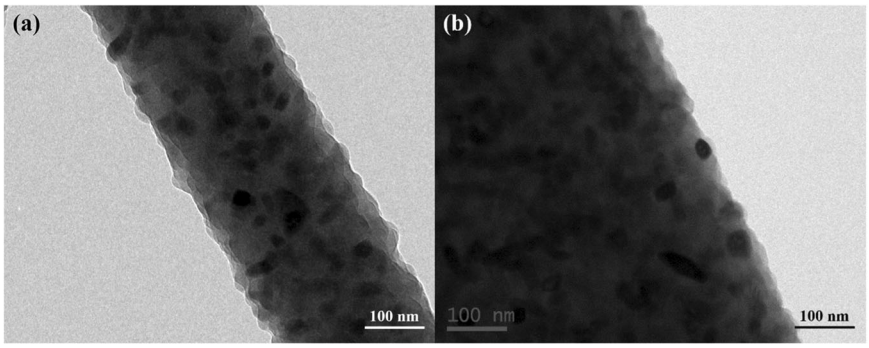

Fig. 9 TEM micrographs of mullite micro/nanofibers prepared at 1200 °C: **a** NF_{S1} and **b** NF_{S4}

As seen, these parameters for NF_{S1} to NF_{S4} decreased accordingly, which was a strong evidence that Si is incorporated into $Al_4B_2O_9$. As concluded above, Si element in fibers prepared using sols with higher concentration possessed the worse dispersion. In this case, the solid solution of Si into the alumina borate structure was hindered, therefore leading to the decrease of the lattice parameters and unit cell volumes.

In Fig. 7b, fibers prepared at 1200 °C were comprised of the $Al_{18}B_4O_{33}$ phase (Card No. 32-0003), mullite phase (Card No. 15-0776) and amorphous SiO_2 [19]. To our knowledge, the XRD patterns of the two crystal phases are similar. The main difference is that the relative intensities of the diffraction peaks at the 2θ of about 26° and 16° reversed. The $I_{0.34}/I_{0.54}$ value for $Al_{18}B_4O_{33}$ was 0.5 and that for mullite was 2. As seen in Fig. 8, these values for fibers prepared at 1200 °C were all in the range of 0.5 to 2. Though a slight decrease tendency was found, ascertaining the form of solid solution was still difficult because the accurate contents of the two crystal phases were unable to be calculated. Due to the formation of mullite phase, it was possible that mullite incorporated with B and $Al_{18}B_4O_{33}$ incorporated with Si coexisted in the fibers.

Figure 9 shows the TEM microstructure of mullite micro/nanofibers prepared using different precursor sols after sintering at 1200 °C. For NF_{S1} exhibited in Fig. 9a, the fiber surface became rough due to the grain growth. The grains possessed sizes ranged from 10 to 90 nm and a mean size of about 50 nm. As to NF_{S4} displayed in Fig. 9b, the grain sizes were in the range of 20 to 110 nm and the mean value of about 70 nm were obviously larger than that of NF_{S1}. According to the above results, amorphous SiO_2 was evenly distributed in fibers derived from precursor sol S1. In fact, it could not only delay the reaction between Al_2O_3 and B_2O_3, but also hinder the movement of grain boundaries. This was responsible for the smaller grains for fibers prepared using sols with a lower concentration.

In summary, the sol concentration was an important factor that affected the microstructure of boron-containing mullite micro/nanofibers. The main reason for its impact was that an amorphous phase existed during the crystallization process. Therefore, it should be noted that oxides micro/nanofibers in mono or binary systems might display different changes when the sol concentration varied, which would be studied further.

4 Conclusion

Boron-containing mullite micro/nanofibers derived from monophasic sols with different concentrations were synthesized via electrospinning. With the concentration increased from 15 to 37.5%, the chemical homogeneity of the precursor sol decreased. As to the spinning solutions, the viscosities and conductivities increased, while the surface tensions decreased. The viscosities played a dominant role in affecting the diameters of the precursor fibers. The fibers prepared using sols with higher concentration possessed the larger diameter shrinking percentage after sintering. The fibers sintered at 900 °C were consisted of $Al_4B_2O_9$ and amorphous SiO_2, and those prepared at 1200 °C were comprised of $Al_{18}B_4O_{33}$, mullite and amorphous SiO_2. Additionally, the decrease in crystallization temperatures and the increase in grain sizes were caused by the more uniform distribution of amorphous SiO_2.

Acknowledgements This work was supported by the Science and Technology Program for Youth Growth of Science and Technology Agency of JiLin Province (No. 20210508055RQ), the Natural Science Foundation of Jilin Province (No. 20210101135JC), the Fund of Education department of JiLin Province (No. JJKH20210733KJ, JJKH20210732KJ) and the JiLin Scientific and Technological Development Program (YDZJ202201ZYTS669).

Compliance with ethical standards

Conflict of interest The authors declare no ompeting interests.

References

1. Xu C, Wang H, Song J et al. (2017) Ultralight and resilient Al_2O_3 nanotube aerogels with low thermal conductivity. J Am Ceram Soc 101:1677–1683

2. Si Y, Wang X, Dou L et al. (2018) Ultralight and fire-resistant ceramic nanofibrous aerogels with temperature-invariant superelasticity. Sci Adv 4:eaas8925
3. Wang H, Zhang X, Wang N et al. (2017) Ultralight, scalable, and high-temperature–resilient ceramic nanofiber sponges. Sci Adv 3:e1603170
4. Su L, Wang H, Niu M et al. (2018) Ultralight, Recoverable, and High-Temperature-Resistant SiC Nanowire Aerogel. ACS Nano 12:3103–3111
5. Dong X, Liu J, Li X et al. (2017) Electrospun mullite nanofibers derived from diphasic mullite sol. J Am Ceram Soc 100:3425–3433
6. Schneider H (2005) Crystal Chemistry of Mullite and Related Phases. In: Schneider H, Komarneni S (Eds.) Mullite. Wiley-VCH, Weinheim, p 1–128
7. Dong X, Chen Z, Guo A et al. (2018) Mechanical and interfacial behavior of single mullite fiber and mullite fiber-based porous ceramics. Ceram Int 44:14446–14456
8. Kim J-H, Yoo S-J, Kwak D-H et al. (2014) Characterization and application of electrospun alumina nanofibers. Nanoscale Res Lett 9:44
9. Tuttle RW, Chowdury A, Bender ET et al. (2008) Electrospun ceramic fibers: Composition, structure and the fate of precursors. Appl Surf Sci 254:4925–4929
10. Wen Z, Song X, Chen D et al. (2020) Electrospinning preparation and microstructure characterization of homogeneous diphasic mullite ceramic nanofibers. Ceram Int 46:12172–12179
11. Wu J, Lin H, Li J et al. (2009) Fabrication and characterization of electrospun mullite nanofibers. Mater Lett 63:2309–2312
12. Wu J, Lin H, Li J et al. (2010) Synthesis and Characterization of Electrospun Mullite Nanofibers. Adv Eng Mater 12:71–74
13. Zhou J, Sun G, Zhao H et al. (2015) Tunable white light emission by variation of composition and defects of electrospun Al_2O_3–SiO_2 nanofibers. Beilstein J Nanotechnol 6:313–320
14. Chen Z, Zhang Z, Tsai CC et al. (2015) Electrospun mullite fibers from the sol–gel precursor. J Sol-Gel Sci Technol 74:208–219
15. Mohammad Ali Zadeh M, Keyanpour-Rad M, Ebadzadeh T (2013) Synthesis of mullite nanofibres by electrospinning of solutions containing different proportions of polyvinyl butyral. Ceram Int 39:9079–9084
16. Mohammad Ali Zadeh M, Keyanpour-Rad M, Ebadzadeh T (2014) Effect of viscosity of polyvinyl alcohol solution on morphology of the electrospun mullite nanofibres. Ceram Int 40:5461–5466
17. Wei H, Li H, Cui Y et al. (2017) Synthesis of flexible mullite nanofibres by electrospinning based on nonhydrolytic sol-gel method. J Sol-Gel Sci Technol 82:718–727
18. Cividanes LS, Campos TMB, Rodrigues LA et al. (2010) Review of mullite synthesis routes by sol-gel method. J Sol-Gel Sci Technol 55:111–125
19. Song X, Liu W, Xu S et al. (2018) Microstructure and elastic modulus of electrospun Al_2O_3-SiO_2-B_2O_3 composite nanofibers with mullite-type structure prepared at elevated temperatures. J Eur Ceram Soc 38:201–210
20. Song X, Liu W, Wang J et al. (2018) Highly aligned continuous mullite nanofibers: Conjugate electrospinning fabrication, microstructure and mechanical properties. Mater Lett 212:20–24
21. Li D, McCann JT, Xia Y, Marquez M (2006) Electrospinning: A simple and versatile technique for producing ceramic nanofibers and nanotubes. J Am Ceram Soc 89:1861–1869
22. Song X, Song Y, Wang J et al. (2020) Insights into the pore-forming effect of polyvinyl butyral (PVB) as the polymer template to synthesize mesoporous alumina nanofibers via electrospinning. Ceram Int 46:9952–9956
23. Song X, Zhang K, Song Y et al. (2020) Morphology, microstructure and mechanical properties of electrospun alumina nanofibers prepared using different polymer templates: A comparative study. J Alloy Compd 829:154502
24. Wang J, Liu W, Song X et al. (2018) Effects of added polyvinyl pyrrolidone on morphology and microstructure of multiple-phase mullite nanofibers. Ceram Int 44:15418–15427
25. Chen L, Wang B, Liu S et al. (1996) Preparation of Mullite Fiber. J Am Ceram Soc 79:1496–1498
26. Voll D, Angerer P, Beran A, Schneider H (2002) A new assignment of IR vibrational modes in mullite. Vib Spectrosc 30:237–243
27. Oréfice R, Vasconcelos W (1997) Sol-Gel transition and structural evolution on multicomponent gels derived from the alumina-silica system. J Sol-Gel Sci Technol 9:239–249
28. Dai Y, Liu W, Formo E et al. (2011) Ceramic nanofibers fabricated by electrospinning and their applications in catalysis, environmental science, and energy technology. Polym Adv Technol 22:326–338
29. Song X, Liu W, Wang J et al. (2017) Microstructural differences between electrospun alumina borate nanofibers prepared by solutions with different PVP contents. Ceram Int 43:9831–9837
30. Song X, Liu J, Wang J et al. (2019) Non-isothermal crystallization kinetics for electrospun $3Al_2O_3{\cdot}B_2O_3{\cdot}2SiO_2$ ceramic nanofibers prepared using different silica sources. Ceram Int 45:1392–1399
31. Griesser KJ, Beran A, Voll D, Schneider H (2008) Boron incorporation into mullite. Miner Pet 92:309–320
32. Zhang G, Fu Z, Wang Y et al. (2010) Boron-doped mullite derived from single-phase gels. J Eur Ceram Soc 30:2435–2441